HHS Public Access

Author manuscript

J Phys Chem B. Author manuscript; available in PMC 2016 July 14.

Published in final edited form as:

J Phys Chem B. 2015 October 22; 119(42): 13309–13320. doi:10.1021/acs.jpcb.5b06838.

Computational Design of Oligopeptide Containing Poly(ethylene glycol) Brushes for Stimuli-Responsive Drug Delivery

Francesca Stanzione and **Arthi Jayaraman***

Department of Chemical and Biomolecular Engineering, University of Delaware, 150 Academy Street, Newark, Delaware 19716, United States

Abstract

Stimuli-responsive biomaterials are used to facilitate drug and gene delivery by shielding the drug/gene during circulation times and selectively releasing the cargo at the desired target. Within stimuli-responsive materials, pH-responsive materials are exploited for delivery to specific organs, intracellular compartments, cancer cells, site of inflammation or infection as those sites are characterized by pH that is different from the blood pH. In this paper we use molecular dynamics (MD) simulations to design such pH-responsive biomaterials where the balance between the various intermolecular interactions (e.g., electrostatics, van der Waals) within the biomaterials allow biofunctional molecules to be reversibly shielded and exposed to the environment with change in pH. In our model the shielding aspect is imparted by a polyethylene glycol (PEG) brush and the pH-responsive component is a PEG-tethered oligopeptide that undergoes changes in conformations via protonation of residues upon changes in pH. Starting with a PEG-tethered peptide in a monodisperse short PEG brush, we first vary the composition and sequence of histidine (H), lysine (K), and glutamate (E) along the oligopeptide sequence to find the design parameters that maximize the shielding and exposure of the oligopeptide at pH ~ 7.0 and pH < 7.0, respectively. Then, we probe the effect of the PEG brush on the conformations of the oligopeptides by simulating PEG-tethered peptide in a bimodal PEG brush containing short PEG and long PEG chains. We characterize the intermolecular interactions involving the PEG, peptide, and solvent that influence the shielded and exposed conformations of the oligopeptides at the two different pHs. In a short monodisperse PEG brush, with a longer PEG-tethered peptide containing large blocks of histidines that undergo change in protonation state as a response to pH change, placed between a protonated lysine and deprotonated glutamate, the PEG brush exhibits maximum shielding and exposure with pH change. This change from shielded to exposed state is driven by electrostatic repulsion upon H protonation. The presence of long PEG chains in a bimodal PEG brush leads to dominating PEG–peptide attractive interactions that reduces the contrast in shielded and exposed conformations of the PEG-tethered peptide upon protonation of histidines.

* arthij@udel.edu. Phone: +1 (302) 831 8682.

Notes

The authors declare no competing financial interest.

Supporting Information

The Supporting Information is available free of charge on the ACS Publications website at DOI: 10.1021/acs.jpcb.5b06838.

Additional intra- and intermolecular interaction energies, the $\langle R_{ee}^2 \rangle^{1/2}$, ⟨SASA⟩, and ΔR_{ee} of pH-responsive peptides, peptide density profiles, and representative simulation snapshots (PDF)

Graphical Abstract

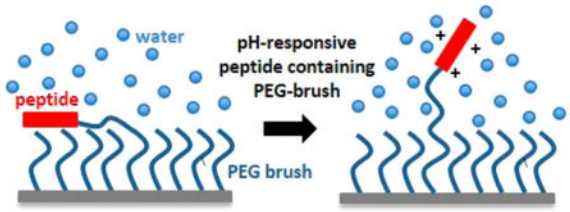

I. INTRODUCTION

Over the past few decades the field of nanomedicine has paid significant attention to engineering optimal biocompatible nanoscale drug carriers.[1] These nanocarriers are made from lipids (e.g., liposomes, nanoemulsions, and solid-lipid nano-particles) and self-assembling amphiphilic biocompatible polymers of varying chemistry and architecture (e.g., linear, dendrimers, comb polymers).[1–9] Incorporation of stimuli-responsive materials within the nanocarriers offers unique features for drug and gene delivery by making the carrier an active participant, rather than a passive vehicle, allowing for targeted delivery. The stimuli-responsive carriers shield the drug during circulation, and expose/deliver them at the target upon being triggered by some stimuli present only at the target (e.g., diseased) site, thus avoiding nonspecific cell and/or tissue biodistribution, and overcoming rapid metabolism or excretion from the body.

The shielding aspect of the stimuli-responsive carrier is often imparted by the use of polyethylene glycol (PEG),[10] a biocompatible polymer that has both hydrophilic and hydrophobic properties. Due to its nontoxic and hydrophilic characteristics, the FDA has approved PEG for use in a wide variety of foods, cosmetic products and pharmaceuticals. When chemically grafted or simply adsorbed on a colloid surface, PEG reduces protein adsorption[11,12] and bacterial adhesion.[13–15] This antiadhesive effect is correlated to high affinity of PEG for water molecules, which creates a hydrated layer that deters adhesion of hydrophobic macromolecule.[16–18]

The targeted delivery aspect of the stimuli-responsive carrier is imparted by incorporating chemistries that are able to recognize and respond to factors such as temperature, pH, ionic strength, electric or magnetic fields, and light within a specific micro-environment.[1–4] Desirable chemistries are ones that undergo a specific protonation, a hydrolytic cleavage, alterations to the hydrophilic/hydrophobic balance, and a molecular or supra-molecular conformational change in response to a stimulus. If a biofunctional group (e.g., active drug) is then encapsulated in the nanocarrier with such stimuli-responsive chemistries, it can be released in response to the specific stimulus[19,20] or it can be linked to the carrier surface and be exposed in response to stimuli.[21–23] The various advances in the design of stimuli-responsive biomaterials are outside the scope of this paper as they have been summarized in several review articles.[1–4]

Within stimuli-responsive biomaterials, pH responsiveness has been exploited to control the delivery of drugs to specific organs, intracellular compartments, cancer cells, sites of

inflammation or infection, all of which are characterized by pH that is different from that of the circulation (blood) pH.[24–26] Two main strategies have been adopted when pH-responsive biomaterials are designed: (a) use of polymers with acid-sensitive bonds whose cleavage enables the release of molecules anchored at the polymer backbone,[23] the modification of the polymer charge or the exposure of targeting ligands, and (b) use of polymers (polyacids or polybases) with ionizable groups that undergo conformational and/or solubility changes in response to environmental pH variation.[22,23] One of the drawbacks or limitations in this design is that the contrast between "stimulus" and "nonstimulus", especially the pH difference between intracellular and extracellular environments, is often small. We can maximize this contrast by optimizing the balance between the various intermolecular forces (e.g., electrostatics, van der Waals) that lead to the functional molecules being reversibly exposed and shielded to the environment in the presence and absence of a stimulus. In this paper we optimize these intermolecular forces in a PEG-tethered peptide polymer brush to maximize the shielded to exposed transition of the PEG-tethered peptide.

In this computational study we focus on a biomaterial consisting of a charged polypeptide tethered to a poly(ethylene glycol) PEG chain in a dense PEG polymer brush, with the possibility of attaching the biofunctional molecule/cargo to the polypeptide (Figure 1a). Our hypothesis is that at physiological pH the balance of the various intermolecular interactions will keep the partially charged polypeptide shielded within the PEG polymer brush, and upon change in pH the completely charged polypeptide will be exposed. By selecting a polypeptide containing lysine (K), glutamic acid (E), and histidine (H) residues, we tune (largely) the electrostatic interactions, and by selecting various features of the PEG brush we tune (largely) the steric interactions (Figure 1b,c). Near physiological pH, although H is weakly pH-sensitive, K is nearly completely positively charged and E is negatively charged. Therefore, the net electrostatic attraction between the positively charged lysines, mostly neutral histidines and negatively charged glutamate residues of the polypeptide at pH = 7–8 will shorten its end-to-end distance, causing the biofunctional molecule that is attached to the peptide to remain buried in the brush. Upon lowering pH < 7, the additional protonated histidines will electrostatically repel like charged lysines/histidines, which will extend the polypeptide chain and push the biofunctional molecule out of the grafted layer. Thus, the specific composition and sequence of the H, E, and K in the polypeptide are two major design "knobs" for the stimuli-responsive PEG brush. On the basis of previous work we hypothesize that a bidisperse polymer brush serves as a route to tailor steric forces that compete with the electrostatic forces to achieve net extensive forces upon subtle changes in electrostatics of the polypeptide chain.[27,28]

These competing intermolecular forces are sensitive to the composition and sequence of amino acids in the peptide chains as well as the molecular weight (MW), grafting density, and polydispersity of the grafted polymers, which constitute far too many parameters than can be tested solely through experiments. This motivates the computational study presented in this paper. The key result is that, whereas the large conformational changes increase with the concentration of H, the relative position of positive and negative amino acids (K and E) in the sequence dictates if they can interact with each other and also dictates how the PEG brush interacts with the oligopeptide. Structurally, comparing the monodisperse PEG brush with bidisperse systems, we observe that the interactions of the peptide with the long PEGs

in the bidisperse brush decreases the exposure of the peptide upon the protonation of H because the peptide interactions with the long PEG chains become the dominant interaction in the system.

The paper is organized as follows. We present the model and methods in section II of this paper. In section III we present our results. We present results showing the effect of composition, sequence of H, K, and E and their relative position on peptide shielding and exposure in two different protonation states of H in a monodisperse 5mer PEG brush. Next, we present the effect of bidisperse PEG brushes on the peptide shielding and exposure by simulating PEG-tethered peptides in 5mer PEG brush surrounded by long PEG chains (10mer and 20mer). Lastly, we examine the effect of varying extents of bidispersity within the PEG brush on the peptide conformational shift by simulating different graft densities of long PEG 20mers surrounding the PEG-tethered peptide. We conclude with a summary of results and potential impact of this work.

II. COMPUTATIONAL METHOD

A. System Studied

We perform atomistic molecular dynamics simulation of PEG polymer brush containing short 5mer PEG chains, long 10mer or 20mer PEG chains, and an oligopeptide tethered to a 10mer PEG spacer (or tether). Our systems represent the surface of the desired pH-responsive polymer brush where the pH-sensitive oligopeptide is tethered to the PEG surface (Figure 1b). The oligopeptide consists of lysine (K), glutamic acid (E), and histidine (H), with equal number of K and E, and varying amounts of K, E, and H in a range of sequences (Table 1). At pH ~ 7 the lysines are protonated (positively charged), the glutamates are negatively charged, and the histidines are mostly neutral. In our model at conditions mimicking pH < 7 all the histidines are also positively charged in addition to the positively charged lysines and negatively charged glutamates. We use H++ computational software (http://biophysics.cs.vt.edu/H++)[29] to predict the pK_a values of the H residue in the peptide sequences, and the pK_a of histidine residues for the sequences discussed in our work is found to be between 5.3 and 6.

To systematically vary the steric effects arising primarily from the PEG brush, we consider a monodisperse 5mer PEG brush and bidisperse PEG brushes with 2, 4, or 8 long (10mer or 20mer) PEG chains amidst a dense layer of short 5mer PEGs. The 2, 4, and 8 long PEG chains are placed at a 1 ± 0.1 nm distance from the PEG-tethered peptide, corresponding to long PEG surface grafting density of approximately 0.6, 0.9, and 1.3 chains/nm^2 (Figure 1c).

B. Simulation Protocol

The peptide sequences are built with PyMol software.[30] The N-terminal residue (exposed end) of the peptide sequences is capped with CH_3–CO group to ensure the neutrality of the ammonium group. The C-terminal group of the peptide sequences (tethered end) is linked to a 5mer PEG spacer/tether chain that is used to covalently link the peptide to the PEG surface. This results in a PEG spacer of 10mer length attached to the peptide amidst a dense monodisperse 5mer PEG brush. The monodisperse PEG brush surface consists of 144 chains

of 5mer PEGs on a 5.25 nm by 5.25 nm by 3.06 nm surface. To immobilize the PEG chains on the surface, the terminal OH groups of the PEGs are restrained in their (x, y, z) positions with a harmonic force constant of 1000 kJ/mol nm^2. In the bimodal/bidisperse brushes, additional long PEG chains (10 and 20mer) are linked to the PEG surface and placed around the PEG-tethered peptide as described in the previous section. The systems are inserted in a triclinic box and then solvated with water and neutralizing counterions (in appropriate cases). To prevent the formation of a second water/PEG interface in the z-direction, we used a long dimension of the box in the z-dimension to avoid interactions between the periodic images.

All molecular dynamics simulations are carried out using GROMACS simulation package, version 4.6.7.[31] The force field used to represent the PEG and peptides is a modified version of the Gromos53a6 force field (Gromos53a6_OXYD), which has been specifically parameterized to reproduce both the structural and thermodynamic properties of peptides and of medium and long PEG chains in polar and weakly polar environments.[32–36] For water we use an SPC force field that is well parameterized with the Gromos53a6 force field, and it is able to reproduce physical and thermodynamic properties of water, such as density, enthalpy of vaporization, radial distribution functions, energies of hydration, and dipole moment.[37] The nonbonded Lennard-Jones interactions within the cutoff (1 nm) are determined between a central atom and the atoms stored in a group neighbor list. Long-tail dispersion corrections are treated analytically. Nonbonded interactions between atoms separated by three or fewer bonds within one molecule are not present, as these effects have been incorporated into the angle and torsional potential parameters. A simulation time step of 2 fs is used with all bond lengths constrained via the LINCS algorithm.[38] We use the Ewald summation technique for calculating the electrostatic interactions. However, because these interfacial systems are not periodic in one of the three dimensions (the z-dimension), we apply a commonly used modified version of the 3D Ewald summation technique to calculate the long-range Coulombic forces.[39] In this modified 3D Ewald summation approach, the reciprocal sum is still performed in 3D, but a correction term is applied for the slab geometry in the z-dimension. The insertion of the correction term ensures results comparable to the 2D Ewald summation, without the insertion on artifact.[40,41]

All systems are subject to energy minimization steps by the steepest descent algorithm.[42] After the initial minimization, the systems are first equilibrated for 1 ns at 300 K and then for another 2 ns at 1 bar to equilibrate water molecules. The production simulations are performed in the NVT ensemble at 300 K using the Berendsen thermostat[43] with a temperature sampling coefficient of 1 ps^{-1}. The production run consists of 200 ns, and only the last 50 ns are used for the data analysis. The configurations in these production runs are stored every 2500 steps (5 ps), ensuring negligible statistical correlation between successive stored configurations. Visualization of the trajectories is performed using Visual Molecular Dynamics (VMD).[44]

C. Analyses

We quantify the conformations of the pH-responsive peptides in the two different protonation states of histidine residues and for various PEG brush features. To quantify the

exposed/shielded conformations of the peptides in different protonation states of H, we calculate three quantities.

i. Average Root Mean Squared End–End Distance ($\langle R_{ee}^2 \rangle^{1/2}$) of the PEG-Tethered Peptide—This is the distance between one peptide end represented by the Cα atom of the N-terminal residue (exposed end) and the other end at C-terminal (tethered end) represented by the N atom of the PEG tether. We also calculate the ΔR_{ee} upon the protonation of H. The error bars in the $\langle R_{ee}^2 \rangle^{1/2}$ plots are the standard deviation calculated from 10 000 configurations collected every 5 ps during the last 50 ns of the simulations.

ii. Average Solvent Accessible Surface Area ($\langle SASA \rangle$) of the Peptide—The shielding/exposure of the peptide to the water is quantified by the solvent accessible surface area (SASA) of the peptide at equilibrium using the Connolly method.[45] The SASA is represented by the contact surface created when a spherical probe of 0.14 nm radius (representing the "solvent") is rolled over the molecular model, and the value of $\langle SASA \rangle$ is reported in this work in terms of the number of such solvent molecules that can roll on the surface of the peptide. In general, it consists of all the points of the van der Waals surface that a solvent sphere can be in contact with. The error bars in the plot are the standard deviation calculated by dividing the last 50 ns of the simulation into 5 blocks of 10 ns time steps and taking the average over these blocks.

iii. Density Profile Perpendicular to the Surface for PEG-Tethered Peptides—The density profile represents the mass per unit volume at a distance (z) from the PEG surface. This is calculated to evaluate the features of the PEG brush and peptide sequences with the largest shift in the peptide density away from surface upon protonation of H. The density distributions are collected from 10 000 snapshots during the last 50 ns of the simulations.

Additionally, the electrostatics and van der Waals interaction energies are also evaluated to quantify the intermolecular attractions and repulsions between various species in the systems. We conduct these pairwise calculations on atoms within the selected species (e.g., within a peptide or peptide and surface) within the cutoff distances set for the interaction potentials. The error bars in these energy plots are the standard errors based on block averages over 5 blocks of 10 ns timesteps/block.

On the basis of the above analyses, we identify the design parameters that produce short $\langle R_{ee}^2 \rangle^{1/2}$ distance, small $\langle SASA \rangle$, and high peptide density near the PEG surface in unprotonated H (for highest shielding), and large increases in $\langle R_{ee}^2 \rangle^{1/2}$ and $\langle SASA \rangle$ and shifts in peptide density away from the surface at protonated H conditions (for largest exposure). We then connect that to the intermolecular interactions that govern the structural trends.

III. RESULTS AND DISCUSSION

A. Effect of Peptide Composition and Sequence in the Absence of Long PEG Chains or Monodisperse PEG Brush

In Figure 2a,b going from sequence 1 to 3, the change in $\langle R_{ee}^2 \rangle^{1/2}$ and ⟨SASA⟩ going from the unprotonated H state to the protonated H state is highest for sequence 2 and comparable for sequences 1 and 3. Table 2 presents the averages and standard deviations shown in Figure 2a,b. Figure 2c shows that in the case of sequences 2 and 1, the PEG-tethered peptide shifts to a farther distance from the PEG surface upon protonation, which is a desirable trait for maximizing exposure upon protonation. Sequence 3 lacks this shift to farther distances from the surface. Figure 3 shows the simulation snapshots that visually describe this quantitative behavior in Figure 2. Sequences 1 and 2 exhibit the types of conformations desirable for a shielded to exposed transition upon protonation of H, but sequence 3 exhibits significant interaction with the PEG surface in both protonated and unprotonated H states.

Figure 4 presents the intra- and intermolecular interactions in these systems that give rise to the structural trends in Figure 3. In the unprotonated H state, the intrapeptide interactions (pep–pep) are the least favorable for sequence 1 among all sequences, because the PEG brush and PEG tether interact with both the neutral H block and positively charged KK in sequence 1. The electrostatic attraction between PEG and positive charges is not surprising because it is well-known that PEG acts as a polyelectrolyte, associating with cations.[46] Indeed, PEG, with its weakly hydrogen-bonding ether linkages (O ether and terminal OH), is able to interact with charged amino acids side chains, as K and E, through hydrogen-bonding mechanisms.[47,48]

In contrast, for sequence 2 in the unprotonated state, the interactions between the E− and K+ at the ends of the peptide cause the peptide to fold, and the pep–pep interactions show the most favorable electrostatics and vdW energies of the three sequences in unprotonated states.

Although pep–PEG surface (pep–Surf) and peptide–solvent (pep–SOL) electrostatic interactions are the same for sequences 1 and 2, the pep–PEG_{tether} electrostatic interactions quantify that the KKEE at the one end of sequence 1 interacts favorably with the PEG tether, but such interactions are not observed in sequence 2. In sequence 3 also there is some E− and K+ interaction (see configurations in Figure 3) leading to an E–K loop, which causes the pep–SOL vdW to be most favorable out of all sequences, and pep–Surf electrostatic interactions to be the weakest for this sequence.

Unlike sequence 2, however, in sequence 3 the PEG tether interacts with the lower half of the peptide, K+, and the neutral HHH block. This interaction is not surprising because, with its methylene groups, PEG is able to form hydrophobic interactions with the uncharged H, stabilizing the conformation of the peptide.[48,49] In the protonated state sequence 1 adopts an upright conformation (Figure 3) because the H block is positively charged and has significant electrostatic repulsion. The pep–Surf and pep–PEG_{tether} interactions become less favorable and pep–SOL more favorable in line with the peptide's upright conformation and with the peptide being exposed. In sequence 2, the favorable E− and K+ interaction that

caused folding in unprotonated state is overwhelmed by the electrostatic repulsion between the charged H in the H block in the peptide. The PEG surface interaction with H+ is also overcome by the electrostatic repulsion, whereas the PEG tether interacts more favorably with the peptide. The exposure to the solvent due to the unfolding of the peptide, leads to strong favorable interactions with the solvent. In sequence 3 the breaking up of H+ block using the intermediate EK (underlined in the sequence) likely helps the PEG interaction with charged H to overcome the electrostatic repulsion caused by protonated HHH. And, this is supported by the pep–Surf electrostatic interactions being more favorable upon protonation for sequence 3 (in contrast to the other 2 sequences). Looking at sequences 2 and 3, we can say that the presence of the EK block along with the placement of the other E and K along the sequence mediate this balance between intrapeptide electrostatic repulsion, intra-peptide attraction, and peptide-PEG interaction.

So far, the peptide sequences with the E and K separated by a large block of H exhibits the largest ΔR_{ee} upon protonation, largest difference in $\langle SASA \rangle$ (thus, largest change in exposure) upon protonation of H along with the lowest $\langle SASA \rangle$ in unprotonated state (most shielded in unprotonated state). This leads us to consider a few other sequences—ones where there is a large block of H with Ks and Es on either end of the peptide (sequences 4a, 4b, 5a, 5b) and all H sequence with no K and E (sequence 6). Sequence 4a and 4b are compositionally the same and differ only in the placement of E and K with respect to the PEG tether. Sequence 4 and 5 differ only in the number of E and K, with sequence 4 having 2 E and 2 K, and sequence 5 having 1 E and 1 K.

In Figure 5, at first glance we see that sequences 4a and 4b are worse than sequence 2 in both the $\langle R_{ee}^2 \rangle^{1/2}$ and $\langle SASA \rangle$ data. Not surprisingly, sequences 4a and 4b are opposite in their behavior, noting the importance of variable PEG tether/surface and water interactions with E and K. Snapshots and peptide density profile in Figure 6 provide a better understanding of the conformations adopted by the PEG-tethered peptide for these sequences.

In sequence 4b, the presence of the 2 E− at the exposed end (N-terminal) and 2 K+ at the tethered end (C-terminal) creates a fold; the EE at the exposed end of the peptide has few interactions with water and prefers to interact with the oppositely charged KK, thus being driven to fold while the PEG tether interacts preferably with the positive charged KK. Upon protonation, the peptide unfolds partially, as seen in the increase in $\langle R_{ee}^2 \rangle^{1/2}$. However, the peptide density profile shows the peptide remains close to the PEG surface for both protonated and unprotonated cases, making the $\langle SASA \rangle$ undesirable, especially in the protonated state.

In contrast to sequence 4b, in sequence 4a the 2 E near the PEG tether are sterically covered by the PEG tether and the 2 K at the exposed end instead interact favorably with the water and then with the PEG surface, thus having a lower driving force to fold (see interaction energies in Figure S1 in the Supporting Information). This is seen with an extended configuration and a high $\langle R_{ee}^2 \rangle^{1/2}$ in the unprotonated state. Upon protonation, the block of H is able to cause enough electrostatic repulsion for the chain to be more exposed, as seen

clearly in the peptide density profile. However, because the peptide is highly water exposed in both states (see ⟨SASA⟩ for seq4a), this sequence is also an undesirable design.

On the basis of results for sequence 4b, clearly, having 2 E and 2 K overstabilizes the folded state in sequence 4b. If we have 1 E and 1 K in the sequence and a large block of H sandwiched between them, we could minimize the stabilization of E and K interaction and increase the effect of H electrostatic repulsion. Doing that in sequence 5a and 5b, we see that indeed these sequences are partially folded in the unprotonated states, and more exposed in the protonated states (Figure 6). The peptide density profiles (Figure 6, upper row) show desirable characteristics for both sequences, whereas unprotonated ⟨SASA⟩ is a little high for sequence 5b, indicating reduced shielding in its unprotonated H state.

All of the above leads to an obvious question of what would happen if there were no E and K in the sequence, e.g., a 100% H sequence.

The 100% H peptide in the unprotonated state adopts a supine conformation on the PEG brush with high $\langle R_{ee}^2 \rangle^{1/2}$ due to PEG–neutral H vdW interactions. The ⟨SASA⟩ is higher than the best case so far (sequence 2) because the folded structure in the unprotonated state of sequence 2 reduces the ⟨SASA⟩, which is not the case here in all H. In the protonated state, the 100% H peptide seems similar to sequence 2 with similar $\langle R_{ee}^2 \rangle^{1/2}$ and ⟨SASA⟩. However, because our design goal is to find the peptide that is most shielded in one pH and most exposed in another pH, sequence 2 outperforms this 100% H sequence 6.

The presence of E and K, with the K on the exposed end and E on the tethered end of the peptide, is essential to induce folding in the unprotonated state, and one large contiguous H block or two blocks of H spaced apart with EK is needed to induce a large electrostatic repulsion upon protonation to break apart the fold. This is a consistent pattern in sequence 2 and sequence 5a. In addition, we note, in Figure S2 that switching the position of E (from C-terminal to N-terminal) and K (from N-terminal to C-terminal) in sequence 2 deteriorates its performance.

B. Effect of Length of Longer PEG Chains Surrounding the PEG-Tethered Peptide on Its Conformation

So far we have presented results for a system with the PEG-tethered peptide being the one long chain amidst a shorter monodisperse PEG brush. Next, we investigate if adding long PEG chains to form a bidisperse brush would enhance or diminish the performance exhibited by the PEG-tethered peptide chain in the previous section.

i. Sequence 1 HHHHHHHHKKEE**—**In the absence of long PEG chains, in the unprotonated state the PEG-tethered peptide interacted with the PEG surface, whereas in the protonated state the block of H+ created enough electrostatic repulsion to overcome the peptide–PEG surface interactions. Our hypothesis is that in the presence of long PEG around the PEG-tethered peptide, in the unprotonated state the peptide could make those same interactions with neighboring PEG chains, increasing the $\langle R_{ee}^2 \rangle^{1/2}$ of the PEG-tethered peptide. However, in the protonated state, the interactions with the neighboring PEGs could compete with the H+ electrostatic repulsions within the peptide that facilitated the peptide exposure.

We expect this to depend on the length of the neighboring long PEG. Because the KKEE at the bottom of the peptide near the PEG surface is likely not seeing a big difference being surrounded by 10mer PEG (PEG_{10}) and by 20mer PEG (PEG_{20}), any effects brought about by adjacent long PEGs are likely dominated by the H block interactions with the PEG. We observe in the snapshots in Figure 7 that the PEG_{20} submerges the sequence in both the unprotonated and protonated H states, confirmed by $\langle R_{ee}^2 \rangle^{1/2}$ data, and less favorable solvent–peptide interaction (Figures S3 and S4); thus the PEG_{20} interactions with the peptide overwhelm the H+ repulsion. This is not the case for PEG_{10}; in the protonated H states where the $\langle R_{ee}^2 \rangle^{1/2}$ is larger with PEG_{10} than with no long PEG. This emergence and exposure of the peptide from the PEG_{10} surrounding layer is also seen with the ⟨SASA⟩ being high, with the pep–SOL electrostatic interactions becoming most favorable (Figure S4) and with the pep–PEG_{10} interactions becoming less favorable. Nonetheless, on the basis of the peptide density profiles (Figure 7), we conclude that both PEG_{20} and PEG_{10} reduce the conformational contrast between the unprotonated state and protonated H state for this sequence 1.

ii. Sequence 2 KHHHHEKHHHHE**—**In the absence of long PEG chains, the interactions of the E− and K+ in the unprotonated state lead to a folded conformation, providing maximum shielding in unprotonated state. And, upon protonation of H the electrostatic repulsion due to charging of the H block leads to unfolding and a large exposure of the peptide. We expect that the length of surrounding PEGs will dictate how and if the PEG chains interact with the K+ and protonated/unprotonated H. Snapshots in Figure 8 and data in Figure S3 show that in the case of PEG_{10} the change in $\langle R_{ee}^2 \rangle^{1/2}$ and the change in ⟨SASA⟩ upon protonation of H is negligible. We do not see a folded state because the PEG_{10} chains interact with the positive K in both unprotonated and protonated state (pink circles in the snapshots in Figure 8). This is also seen in the intermolecular interactions where the value of the pep–PEG_{10} interactions is favorable with surrounding PEG_{10}, in both protonated and unprotonated states, compared to other sequences (Figure S4).

PEG_{20} buries the peptide in unprotonated and protonated states (Figure 8). The extended state of the peptide in the protonated state versus the unprotonated state is brought about by favorable peptide (vdW and electrostatic) interactions with PEG_{20} in the protonated state than in the unprotonated state (Figure S4). Therefore, likely when the peptide is in an extended conformation, the PEG_{20} chains are able to make more favorable contacts with the various H+ blocks along the peptide chain and with the K+ at the exposed end of the peptide, while minimizing H+ block repulsions.

The peptide density profiles (Figure 8) further confirm that addition of eight long PEG chains reduces the exposure in the protonated states, and makes this sequence less desirable in the presence of bimodal PEG brush.

iii. Sequence 3 EHHHKHHEKHHH**—**In the absence of long PEG chains, this peptide formed the K–E loop in the unprotonated state, and in the protonated state the peptide–PEG surface interactions dominated over the H+ electrostatic repulsions as H + were spaced out with the EK in the middle of the sequence. In the presence of PEG_{10}, in the unprotonated state of H, K+ interact with the PEG tether (bringing the peptide closer to the surface). In the

protonated state, the PEG_{10} chains and the PEG tether all interact with H+. Because the H+ is not one contiguous block (like in sequence 1) or a large block (like sequence 2), the electrostatic repulsions from the H+ are not strong enough to overcome these PEG–H+ interactions. These interactions between the H+ and PEGs maintain the peptide farther from the surface but well within the PEG_{10} layers. The interaction energies in Figure S4 show very favorable peptide–PEG_{10} interactions. PEG_{20} behaves in a manner similar to that of PEG_{10} (Figure S4 and S5). We note that in this sequence 3, the addition of long PEGs around the PEG-tethered peptide shifts the peptide density to farther distances from the surface upon protonation than the no long PEG case. However, we do not see improvement in change in SASA (Figure S3) with addition of long PEGs. As shown in snapshots in Figure S5, we see that the long PEG chains simply "lift" the peptide from the PEG surface to better interact with the peptide.

iv. Sequence 6, 100% H—In the unprotonated state, the H exhibit interactions with the PEG surface, PEG tether, and the long PEG (PEG_{10} and PEG_{20}) chains. In the protonated state of H and in the presence of the eight PEG_{10} or eight PEG_{20}, the large electrostatic repulsions within the all-H peptide overcome the PEG–H+ interactions extending the peptide in a manner similar to that of no long PEG (Figure 9). The difference between PEG_{20} and PEG_{10} is that in the protonated state, PEG_{20} has enough PEG monomers to keep the peptide buried close to the surface, whereas the peptide is exposed in the presence of PEG_{10} (see simulation snapshots and peptide density profile in Figure 9).

Thus, for this sequence, although the eight PEG_{10} does not change the desired peptide density profile seen with no PEG (Figure 9), it does increase the solvent exposure ($\langle SASA \rangle$ data in Figure S3) in the unprotonated state compared to no PEG, thus reducing the performance of this sequence with addition of long PEG.

v. Sequence 5a KHHHHHHHHHHE**—**In most cases, the effect of PEG20 on the $\langle R_{ee}^2 \rangle^{1/2}$, $\langle SASA \rangle$, and peptide density profile is similar for this sequence (Figure 10 and Figure S3) and sequence 6. The interaction energies between long PEG and peptide also show the same trend for both sequences 5a and 6. For PEG_{10} the solvent interactions with sequence 6 show a much more favorable change upon protonation than sequence 5a, in agreement with a larger increase in SASA upon protonation for sequence 6. And, to counterbalance, the PEG surface interactions with the peptide become unfavorable/less favorable upon protonation for sequence 6, whereas it remains fairly constant for sequence 5a. This agrees with the lack of shift in peptide density profile for sequence 5a with PEG_{10}, whereas it continues to show some contrast for sequence 6.

So far, in all cases for both PEG lengths, a high grafting density of adjacent long PEG chains in the bimodal distribution only negatively impacts the efficacy of peptide sequence in adopting a shielded conformation in unprotonated H state and exposed conformation in the protonated H state.

C. Effect of Varying Bidispersity within the PEG Brush on the Peptide Conformations

Table 3 presents the $\langle R_{ee}^2 \rangle^{1/2}$ and $\langle SASA \rangle$ for the unprotonated and protonated H states for sequences 1, 2, 3, 5a, and 6, for PEG brushes with 0, 2, 4, and 8 PEG_{20} chains. By studying

systems with 2, 4, and 8 PEG_{20} chains amidst the PEG_5 brush, we are able to show the effect of varying bidispersity/bimodality in the PEG brushes on the performance of peptides.

In most sequences, having 2, 4, and 8 PEG_{20} chains (i) slightly increases (or maintains within error) the SASA from the no long PEG case (Table 3) and (ii) increases the PEG_{20} interactions with the peptide and reduces solvent–peptide interactions particularly in the protonated states compared to the no long PEG case (Figure S7). In all cases the contrast in peptide density profile from the PEG surface between unprotonated and protonated H states decreases in the presence of long PEG_{20} (Figure 11).

i. Sequence 2 KHHHHEKHHHHE**—**In the case of 2 PEG_{20} the peptide density is shifted away from the surface upon protonation, a desirable feature, but not to the same extent as the no PEG case. As grafting density increases, the distribution of the peptide to the surface shifts to larger distances while the difference or contrast in the peptide density profile between the unprotonated and protonated states decreases. As shown in Figure 11, for the 8 PEG_{20} case a non-negligible peptide density distribution at larger distances (black circle) is present upon the protonation of H. In this state, the increased PEG crowding contributes to the extended conformation of the peptide. This extended state for 8 PEG_{20} is not seen for 2 and 4 PEG_{20} cases, in agreement with ΔR_{ee} (Figure S6). This is because upon the protonation of H, the peptide interactions with the solvent are less favorable (opposite of no PEG case) and interactions with PEG_{20} are more favorable (Figure S7).

Because the overall exposure in the protonated state is lower than the no long PEG case, irrespective of grafting density, we conclude that adding the long PEGs is really not improving the performance of this sequence.

ii. Sequence 3 EHHHKHHEKHHH**—**The addition of 2 PEG_{20} improves the design from both the $\langle R_{ee}^2 \rangle^{1/2}$ and ⟨SASA⟩ perspective. Table 3 shows that the main change in ⟨SASA⟩ that the 2 PEG_{20} chains brought the unprotonated state looks fairly similar in ⟨SASA⟩ with 2 PEG_{20} and with no long PEG_{20}. In terms of $\langle R_{ee}^2 \rangle^{1/2}$, the 2 PEG_{20} chains decrease the unprotonated $\langle R_{ee}^2 \rangle^{1/2}$ and increase the protonated $\langle R_{ee}^2 \rangle^{1/2}$ (desired). Visual analysis (Figure S8) shows that while in the no long PEG case the PEG surface interacts with the peptide in the protonated state making the peptide less exposed in the protonated state, in the presence of 2 PEG_{20} chains, the peptide is lifted from the PEG surface and exposed toward the solvent. In contrast 4 and 8 PEG_{20} basically reduce differences between unprotonated and protonated states; this is because the 4 or 8 PEG_{20} maximize the interaction with the positive charges in the peptide by forming numerous loops around the positive residues in the sequence in the protonated states, pulling the peptide to the surface.

IV. CONCLUSION

In this paper we conducted atomistic molecular dynamics simulations of pH-responsive PEG brushes containing oligopeptides to design pH-responsive shielding and exposure of the PEG-tethered peptide, and to understand the effect of the polydispersity in PEG polymer brush, the oligopeptide composition and the sequence of residues H, K, and E on the extent of exposure of PEG-tethered peptide upon protonation of H. We systematically varied the

amount of H residues, and sequence (e.g., blockiness of H residues, placement of E and K residues) to isolate the PEG interaction with the various charged and uncharged residues of the peptide.

We found that in a monodisperse PEG brush, a contiguous block of H residues within the PEG-tethered peptide causes the largest increase in exposure of the PEG-tethered oligopeptide upon the protonation of H due to dominant electrostatic repulsions. The presence of a K residue at the N-terminal and an E residue at the C-terminal of oligopeptide stabilize the folded/shielded conformation in the unprotonated H state due to favorable electrostatic interactions between K^+ and the PEG brush. The presence of an effectively "neutral spacer" EK block within the large block of H residues further creates a point within the peptide to observe folding (shielding) in unprotonated H state.

We also studied how bidisperse PEG brushes impact the above trends. High grafting density of long (20mer) amidst short (5mer) PEG chains, next to the (10mer) PEG-tethered peptide, caused the pH-responsive shielding and exposure of the oligopeptide to decrease in most sequences. This is because the dense surrounding of long PEGs enhanced the interactions with the positive charges located in the peptide sequence. Even though our expectation was that the electrostatic repulsions within the peptide would overcome the electrostatic attraction between peptide–PEG, resulting in a more exposed conformation, we saw that the long PEG interactions with the peptide dominate and reduce the contrast in peptide conformations between the unprotonated and protonated H states. With few long PEG chains (e.g., 2), we observed that the long PEG–peptide interactions were not dominant but replaced the short PEG brush–peptide interaction that stabilized supine conformations, leading to extended conformations of the PEG-tethered peptide in the presence of a few long PEG chains. However, even in these cases the contrast between the shielded and exposed state conformations was decreased. Thus, the choice of monodisperse PEG brush that is shorter than the PEG-tethered peptide lead to the largest contrast in shielded and exposed states.

We also found that in addition to interacting with the residues, the PEG brush and PEG tether affect the ability of the surrounding water to solvate the charged residues. We note that, although in the low salt concentrations (only counterions) considered here these PEG-mediated water–peptide interactions lead to more extended conformations of the peptides, it is possible that at high salt concentrations the differences between the conformations of the PEG-tethered peptides in the unprotonated and protonated H states might be reduced. This is because of the possibility of the peptide and PEG to interact with different ions in solution and/or due to screening of electrostatic interactions that dominate the exposure of the peptide in the protonated H state. A systematic follow up study looking into the effects of various ions and salt concentration will help understand how physiological salt concentration (0.15 M) alters, if at all, the presented results here.

In conclusion, this study shows the delicate interplay/competition of electrostatic interactions between PEG brush with the charged and uncharged residues of peptide versus the intrapeptide interactions, as a function of PEG brush features and peptide composition. This information is valuable in the design of peptide-decorated PEG-based biomaterials,

impacting a wide variety of applications, including tissue engineering scaffolds, drug delivery, gene delivery, etc.

Supplementary Material

Refer to Web version on PubMed Central for supplementary material.

Acknowledgments

This project was financially supported by the Delaware COBRE pilot program, with a grant from the National Institute of General Medical Sciences – NIGMS (1 P30 GM110758-01) from the National Institutes of Health. The authors thank Teragrid/XSEDE (allocation MCB100140) for supercomputing time and the Farber supercomputer supported by the University of Delaware.

References

1. Fleige E, Quadir Ma, Haag R. Stimuli-Responsive Polymeric Nanocarriers for the Controlled Transport of Active Compounds: Concepts and Applications. Adv Drug Delivery Rev. 2012; 64(9): 866–884.
2. Chen J, Chang C. Materials. 2014; 7:805–875.
3. Mura S, Nicolas J, Couvreur P. Stimuli-Responsive Nanocarriers for Drug Delivery. Nat Mater. 2013; 12(11):991–1003. [PubMed: 24150417]
4. Ganta S, Devalapally H, Shahiwala A, Amiji M. A Review of Stimuli-Responsive Nanocarriers for Drug and Gene Delivery. J Controlled Release. 2008; 126(3):187–204.
5. Zhang M, Liu L, Zhao H, Yang Y, Fu G, He B. Double-Responsive Polymer Brushes on the Surface of Colloid Particles. J Colloid Interface Sci. 2006; 301(1):85–91. [PubMed: 16780862]
6. Torchilin VP. Targeted Pharmaceutical Nanocarriers for Cancer Therapy and Imaging. AAPS J. 2007; 9(2):E128–E147. [PubMed: 17614355]
7. Vasir JK, Reddy MK, Labhasetwar VD. Nanosystems in Drug Targeting: Opportunities and Challenges. Curr Nanosci. 2005; 1:47–64.
8. Andresen TL, Jensen SS, Jørgensen K. Advanced Strategies in Liposomal Cancer Therapy: Problems and Prospects of Active and Tumor Specific Drug Release. Prog Lipid Res. 2005; 44:68–97. [PubMed: 15748655]
9. Couvreur P. Nanoparticles in Drug Delivery: Past, Present and Future. Adv Drug Delivery Rev. 2013; 65:21–23.
10. Pasut G, Veronese FM. PEG Conjugates in Clinical Development or Use as Anticancer Agents: An Overview. Adv Drug Delivery Rev. 2009; 61:1177–1188.
11. Montet X, Weissleder R, Josephson L. Imaging Pancreatic Cancer with a Peptide-Nanoparticle Conjugate Targeted to Normal Pancreas. Bioconjugate Chem. 2006; 17(4):905–911.
12. Rissanen S, Kumorek M, Martinez-Seara H, Li Y, Jamroz D, Bunker A, Nowakowska M, Vattulainen I, Kepczynski M, Rog T. J Phys Chem B. 2014; 118:144. [PubMed: 24350646]
13. Kingshott P, Wei J, Bagge-Ravn D, Gadegaard N, Gram L. Covalent Attachment of Poly(ethylene Glycol) to Surfaces, Critical for Reducing Bacterial Adhesion. Langmuir. 2003; 19(17):6912–6921.
14. Park KD, Kim YS, Han DK, Kim YH, Lee EHB, Suh H, Choi KS. Bacterial Adhesion on PEG Modified Polyurethane Surfaces. Biomaterials. 1998; 19(7–9):851–859. [PubMed: 9663762]
15. Wagner VE, Koberstein JT, Bryers JD. Protein and Bacterial Fouling Characteristics of Peptide and Antibody Decorated Surfaces of PEG-Poly(acrylic Acid) Co-Polymers. Biomaterials. 2004; 25(12):2247–2263. [PubMed: 14741590]
16. Harris JM, Struck EC, Case MG, Paley MS, Yalpani M, Van Alstine JM, Brooks DE. Synthesis and Characterization of Poly(ethylene Glycol) Derivatives. J Polym Sci, Polym Chem Ed. 1984; 22(2): 341–352.

17. Kojima C, Kono K, Maruyama K, Takagishi T. Synthesis of Polyamidoamine Dendrimers Having Poly(ethylene Glycol) Grafts and Their Ability to Encapsulate Anticancer Drugs. Bioconjugate Chem. 2000; 11(6):910–917.
18. Zhang Z, Berns AE, Willbold S, Buitenhuis J. Synthesis of Poly(ethylene Glycol) (PEG)-Grafted Colloidal Silica Particles with Improved Stability in Aqueous Solvents. J Colloid Interface Sci. 2007; 310(2):446–455. [PubMed: 17346738]
19. Min KH, Kim JH, Bae SM, Shin H, Kim MS, Park S, Lee H, Park RW, Kim IS, Kim K, et al. Tumoral Acidic pH-Responsive MPEG-Poly(β-Amino Ester) Polymeric Micelles for Cancer Targeting Therapy. J Controlled Release. 2010; 144(2):259–266.
20. Gao GH, Park MJ, Li Y, Im GH, Kim JH, Kim HN, Lee JW, Jeon P, Bang OY, Lee JH, et al. The Use of pH-Sensitive Positively Charged Polymeric Micelles for Protein Delivery. Biomaterials. 2012; 33(35):9157–9164. [PubMed: 23000386]
21. Quan CY, Chen JX, Wang HY, Li C, Chang C, Zhang XZ, Zhuo RX. Core - Shell Nanosized Assemblies Mediated by the A - Bdimer with a Tumor-Triggered Targeting Property. ACS Nano. 2010; 4(7):4211–4219. [PubMed: 20521828]
22. Koren E, Apte A, Jani A, Torchilin VP. Multifunctional PEGylated 2C5-Immunoliposomes Containing pH-Sensitive Bonds and TAT Peptide for Enhanced Tumor Cell Internalization and Cytotoxicity. J Controlled Release. 2012; 160(2):264–273.
23. Lee ES, Gao Z, Kim D, Park K, Kwon IC, Bae YH. Super pH-Sensitive Multifunctional Polymeric Micelle for Tumor pHe Specific TAT Exposure and Multidrug Resistance. J Controlled Release. 2008; 129(3):228–236.
24. Radovic-Moreno AF, Lu TK, Puscasu VA, Yoon CJ, Langer R, Farokhzad OC. Surface Charge-Switching Polymeric Nanoparticles for Bacterial Cell Wall-Targeted Delivery of Antibiotics. ACS Nano. 2012; 6(5):4279–4287. [PubMed: 22471841]
25. Tannock IF, Rotin D. Acid pH in Tumors and Its Potential for Therapeutic Exploitation. Cancer Res. 1989; 49:4373–4384. [PubMed: 2545340]
26. Xia Y, Wang Y, Wang Y, Tu C, Qiu F, Zhu L, Su Y, Yan D, Zhu B, Zhu X. A Tumor pH-Responsive Complex: Carboxyl-Modified Hyper branched Polyether and Cis-dichlorodiammineplatinum(II). Colloids Surf, B. 2011; 88(2):674–681.
27. Martin TB, Jayaraman A. Polydisperse Homopolymer Grafts Stabilize Dispersions of Nanoparticles in a Chemically Identical Homopolymer Matrix: An Integrated Theory and Simulation Study. Soft Matter. 2013; 9(29):6876.
28. Martin TB, Dodd PM, Jayaraman A. Polydispersity for Tuning the Potential of Mean Force between Polymer Grafted Nanoparticles in a Polymer Matrix. Phys Rev Lett. 2013; 110(1)doi: 10.1103/PhysRevLett.110.018301
29. Anandakrishnan R, Aguilar B, Onufriev AV. H++ 3.0: Automating pK Prediction and the Preparation of Biomolecular Structures for Atomistic Molecular Modeling and Simulations. Nucleic Acids Res. 2012; 40 (W1).W537. doi: 10.1093/nar/gks375
30. DeLano, WL. The PyMOL Molecular Graphics System. 2002. on World Wide Web http://www.pymol.org
31. Pronk S, Páll S, Schulz R, Larsson P, Bjelkmar P, Apostolov R, Shirts MR, Smith JC, Kasson PM, Van Der Spoel D, et al. GROMACS 4.5: A High-Throughput and Highly Parallel Open Source Molecular Simulation Toolkit. Bioinformatics. 2013; 29(7):845–854. [PubMed: 23407358]
32. Oostenbrink C, Villa A, Mark AE, van Gunsteren WF. A Biomolecular Force Field Based on the Free Enthalpy of Hydration and Solvation: The GROMOS Force-Field Parameter Sets 53A5 and 53A6. J Comput Chem. 2004; 25(13):1656–1676. [PubMed: 15264259]
33. Fuchs PFJ, Hansen HS, Hünenberger PH, Horta BAC. A GROMOS Parameter Set for Vicinal Diether Functions: Properties of Polyethyleneoxide and Polyethyleneglycol. J Chem Theory Comput. 2012; 8:3943. [PubMed: 26593032]
34. Daura X, Mark AE, Van Gunsteren WF. Parametrization of Aliphatic CHn United Atoms of GROMOS96 Force Field. J Comput Chem. 1998; 19(5):535–547.
35. Fuchs PFJ, Hansen HS, Hünenberger PH, Horta BAC. A GROMOS Parameter Set for Vicinal Diether Functions: Properties of Polyethyleneoxide and Polyethyleneglycol. J Chem Theory Comput. 2012; 8(10):3943–3963. [PubMed: 26593032]

36. Oostenbrink C, Soares TA, Van Der Vegt NFA, Van Gunsteren WF. Validation of the 53A6 GROMOS Force Field. Eur Biophys J. 2005; 34(4):273–284. [PubMed: 15803330]
37. Mark P, Nilsson L. Structure and Dynamics of the TIP3P, SPC, and SPC/E Water Models at 298 K. J Phys Chem A. 2001; 105(43):9954–9960.
38. Hess B, Bekker H, Berendsen HJC, Fraaije JGEM. LINCS: A Linear Constraint Solver for Molecular Simulations. J Comput Chem. 1997; 18(12):1463–1472.
39. Yeh I, Berkowitz ML. Ewald summation for systems with slab geometry. J Chem Phys. 1999; 111(7):3155.
40. Essmann U, Perera L, Berkowitz ML, Darden T, Lee H, Pedersen LG. A Smooth Particle Mesh Ewald Method. J Chem Phys. 1995; 103:8577–8593.
41. Darden T, York D, Pedersen L. Particle Mesh Ewald: An N log(N) Method for Ewald Sums in Large Systems. J Chem Phys. 1993; 98(12):10089.
42. Arfken G. Mathematical Methods for Physicists. Am J Phys. 1972; 40:642.
43. Berendsen HJC, Postma JPM, van Gunsteren WF, DiNola A, Haak JR. Molecular Dynamics with Coupling to an External Bath. J Chem Phys. 1984; 81(8):3684–3690.
44. Humphrey W, Dalke A, Schulten K. VMD: Visual Molecular Dynamics. J Mol Graphics. 1996; 14:33–38.
45. Connolly ML. Analytical Molecular Surface Calculation. J Appl Crystallogr. 1983; 16(5):548–558.
46. Hakem IF, Lal J, Bockstaller MR. Binding of Monovalent Ions to PEO in Solution: Relevant Parameters and Structural Transitions. Macromolecules. 2004; 37(22):8431–8440.
47. Israelachvili J. The Different Faces of Poly (Ethylene Glycol). Proc Natl Acad Sci U S A. 1997; 94:8378–8379. [PubMed: 11607748]
48. Zobnina VG, Kosevich MV, Chagovets VV, Boryak Oa, Vekey K, Gömöry Á, Kulyk AN. Interactions of Oligomers of Organic Polyethers with Histidine Amino Acid. Rapid Commun Mass Spectrom. 2012; 26(5):532–540. [PubMed: 22302493]
49. Sasahara K, Uedaira H. Solubility of Amino Acids in Aqueous Poly (ethylene Glycol) Solutions. Colloid Polym Sci. 1993; 271(11):1035–1041.

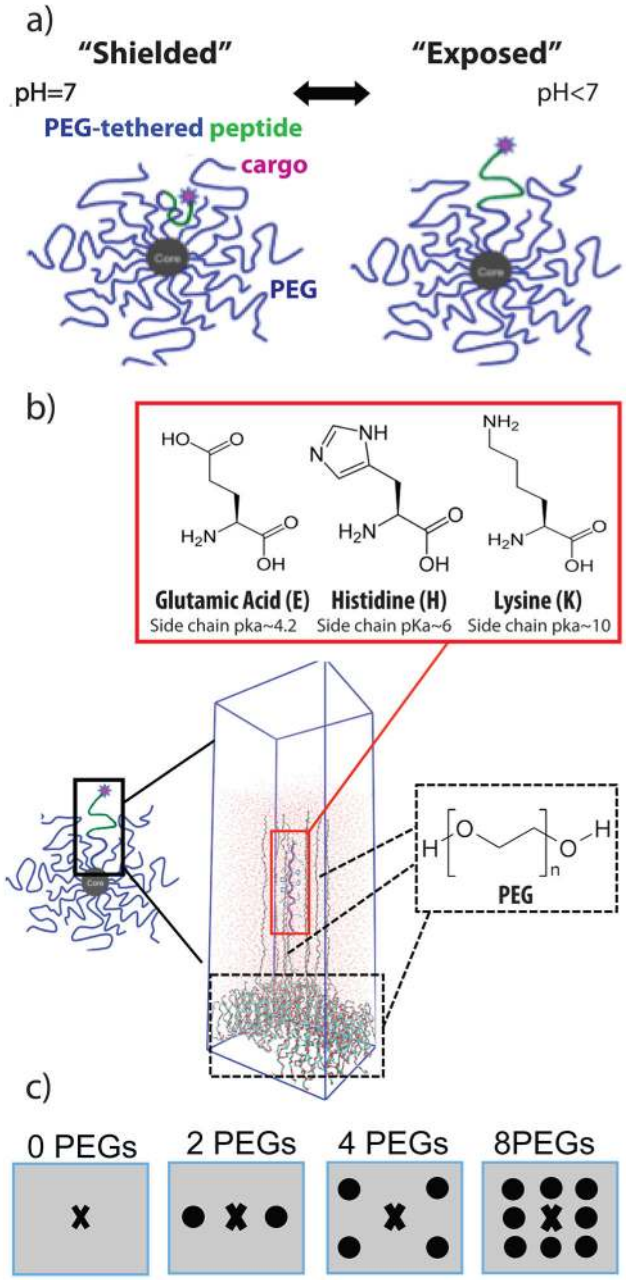

Figure 1.

(a) Schematic of a pH-responsive poly(ethylene glycol) (PEG) brush containing a PEG-tethered peptide with a cargo. The image shows the cargo (purple sphere) in a shielded state at pH = 7 and exposed stated in pH < 7. (b) The part of the PEG brush that we simulate in this paper. Chemical structure of the amino acids in the PEG-tethered peptide are presented on the right. (c) To vary the bidispersity, we vary the number of long PEG chains amidst the short PEG brush; the top view of the location of 0, 2, 4, and 8 long PEG chains are shown, where the long PEG chains are denoted with circles and the PEG-tethered peptide chain on the PEG surface are denoted by a cross.

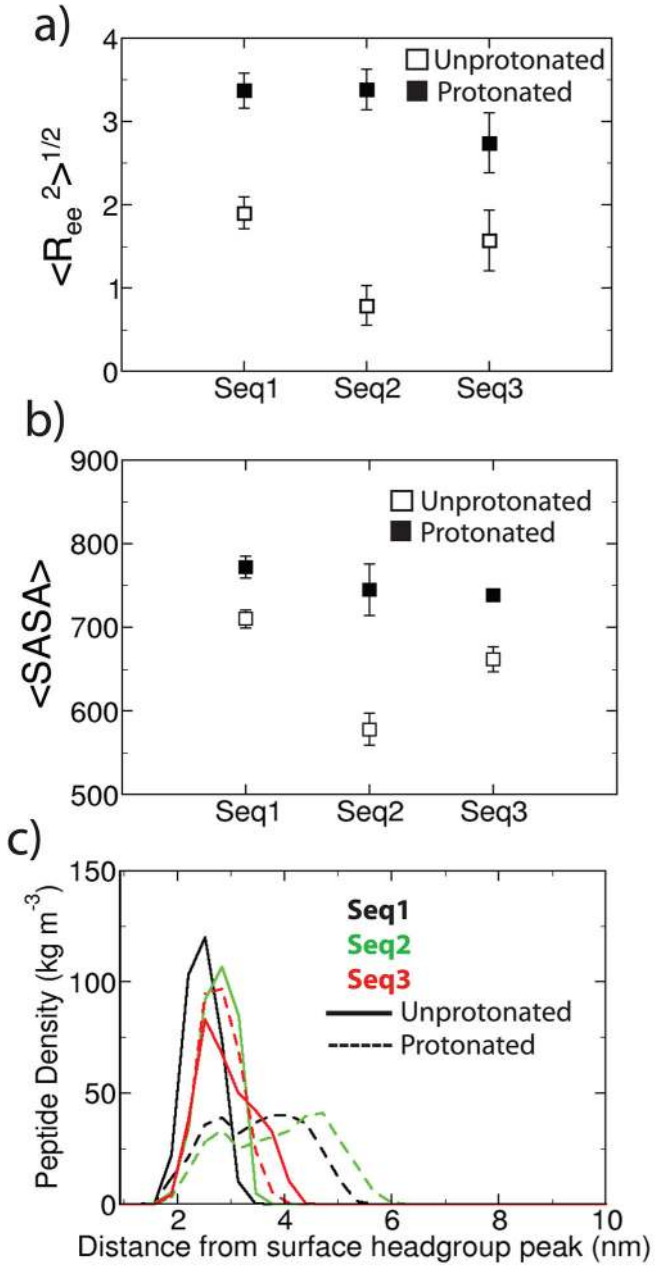

Figure 2.

(a) Average root mean squared end–end distance, $\langle R_{ee}^2 \rangle^{1/2}$, in nm, and (b) average solvent accessible surface area, ⟨SASA⟩, in units of number of water probes of 0.14 nm radius, as a function of sequence for unprotonated (open symbol) and protonated (solid symbols) states. The sequences in *x*-axis are listed in Table 1, and the error bars plotted in the figure are the standard deviations from the average calculated as described in the analysis section. (c) Average peptide density as a function of distance from PEG surface for the unprotonated (solid line) and protonated (dashed line) states for the three sequences 1, 2, and 3 (Table 1). The density distributions are collected from 10 000 snapshots during the last 50 ns of the simulations.

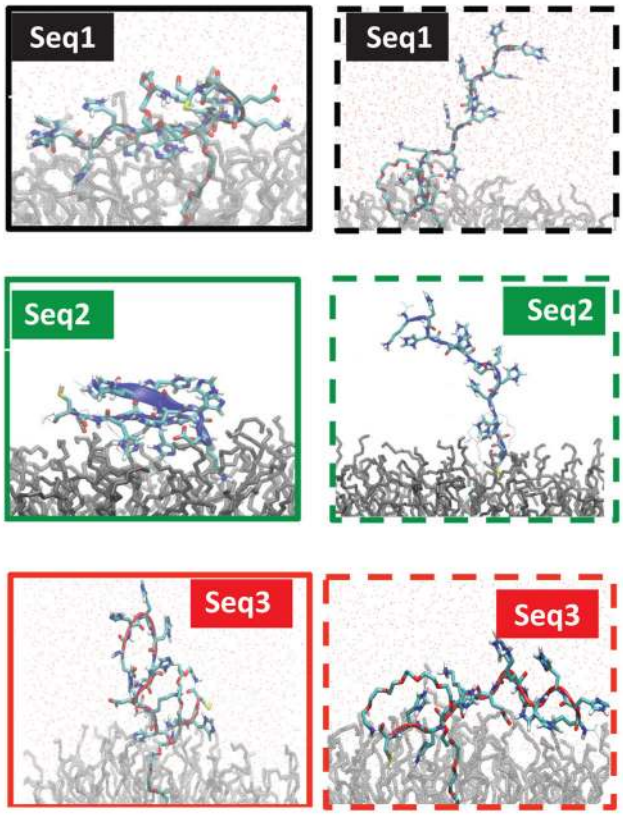

Figure 3.
Representative simulation snapshots of PEG-tethered peptide in unprotonated (left column) and protonated states (right column) for sequences 1, 2, and 3. The water and counterions are hidden for clarity, and only a section of the PEG is shown.

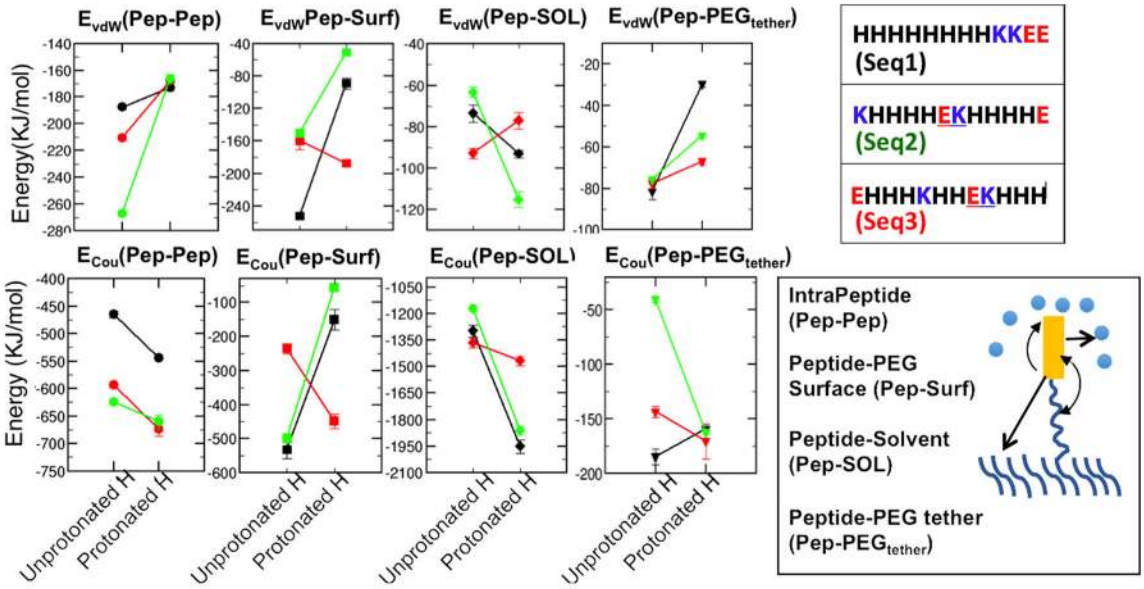

Figure 4.

Intra- and intermolecular interaction energies between various components of the systems. The electrostatic (subscript Cou) and van der Waals (subscript vdW) interactions are shown separately for various pairs. The error bars plotted in the figure are the standard errors of the mean calculated as described in the analysis section. Legends are shown in the right along with a schematic describing the various pairs.

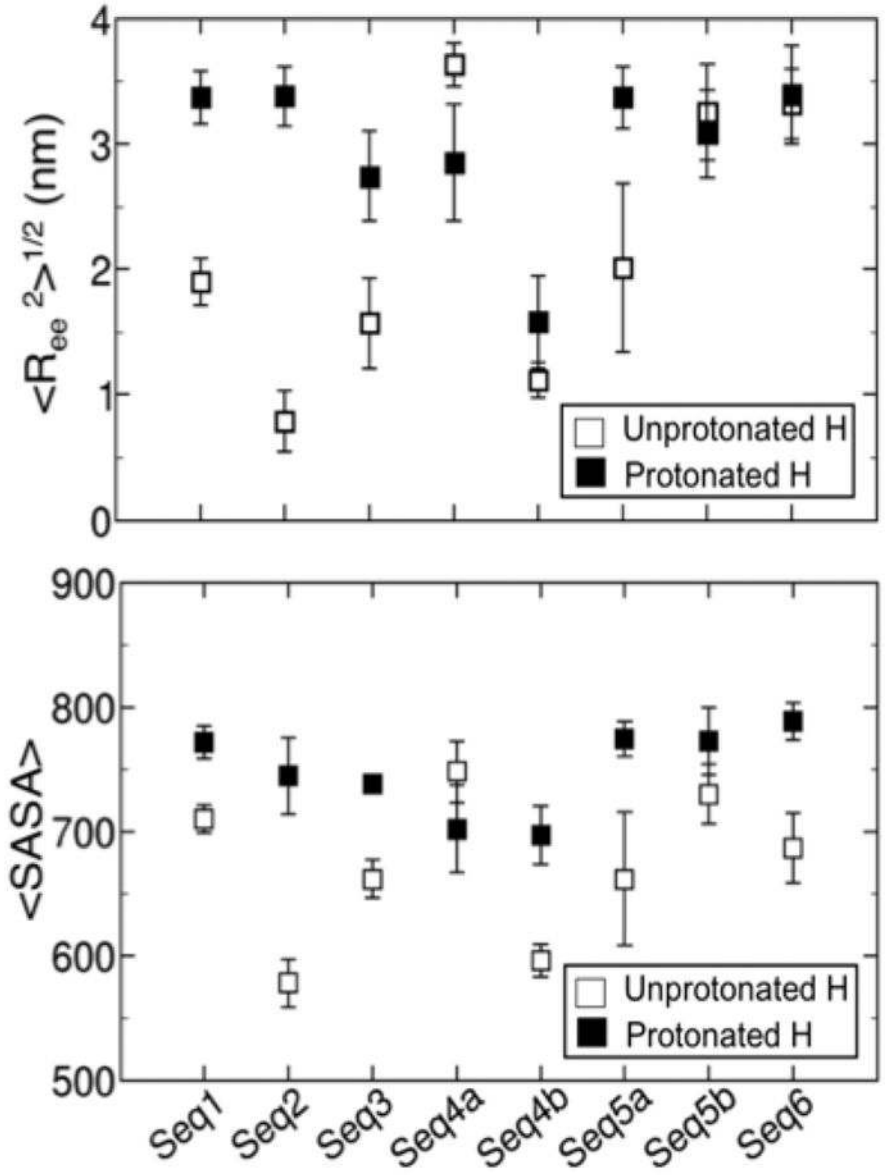

Figure 5.

(Top) average root mean squared end-end distance, $\langle R_{ee}^2 \rangle^{1/2}$, in nm, and (bottom) average solvent accessible surface area, ⟨SASA⟩, in units of water probes of 0.14 nm radius, as a function of sequence for unprotonated (open symbol) and protonated (solid symbol) states. The sequences in the *x*-axis are listed in Table 1, and the error bars are the standard deviations from the average calculated as described in the analysis section.

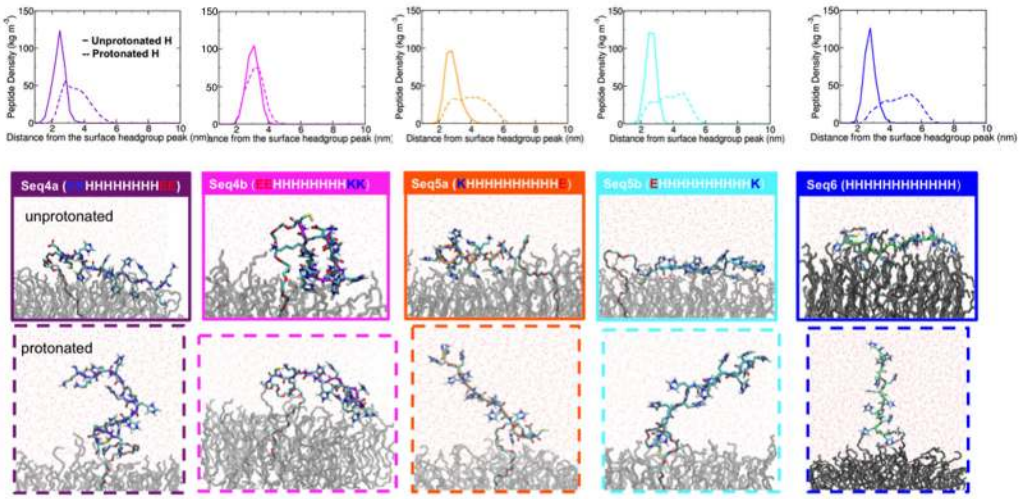

Figure 6.

(Top row) peptide density as a function of distance from the PEG surface for the unprotonated (solid line) and protonated (dashed line) states for the five sequences 4a, 4b, 5a, 5b, and 6 (described in Table 1). (Bottom row) representative simulation snapshots of PEG-tethered peptides in unprotonated and protonated states for sequences 4a, 4b, 5a, 5b, and 6. The water and counterions are hidden for clarity, and only a section of the PEG substrate is shown.

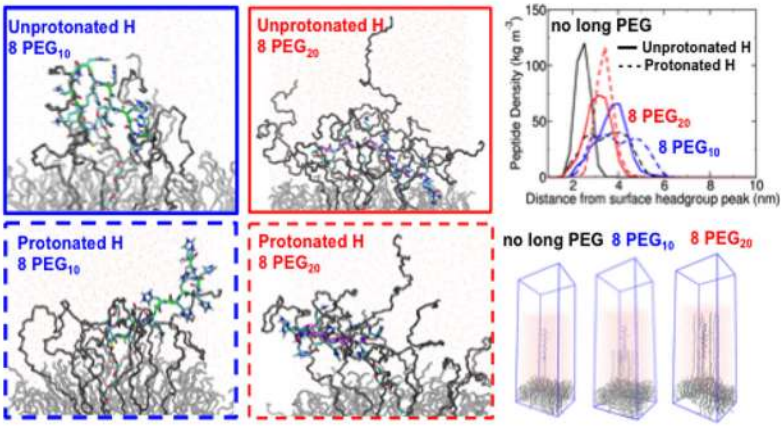

Figure 7.

Representative simulation snapshots of sequence 1 in unprotonated and protonated states. The water and counterions are hidden for clarity, and only a section of the PEG coated substrate is shown. The peptide density profile, as a function of distance from the PEG surface, for the unprotonated (solid line) and protonated (dashed line) states with no long PEG (black), 8 PEG_{10} (blue), and 8 PEG_{20} (red) is also shown.

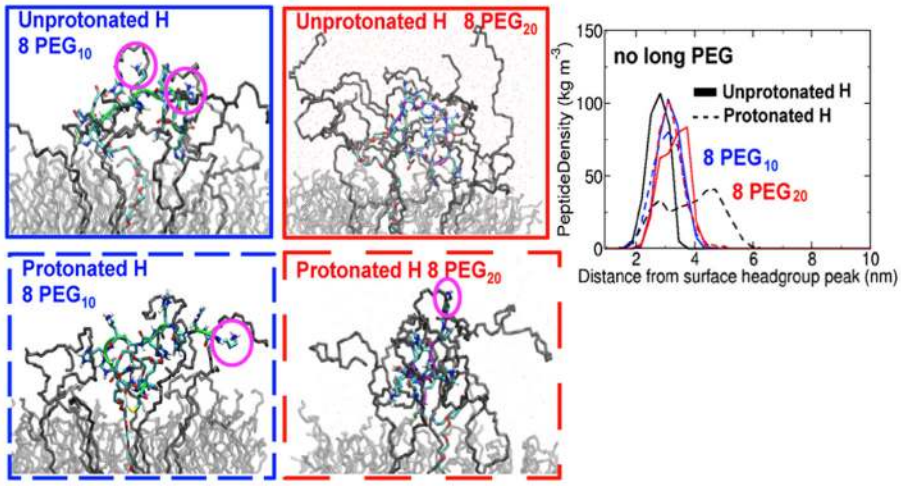

Figure 8.

Representative simulation snapshots of sequence 2 in unprotonated (top row) and protonated (bottom row) states. The water and counterions are hidden for clarity, and only a section of the PEG coated substrate is shown. The peptide density profile, as a function of distance from the PEG surface, for the unprotonated (solid line) and protonated (dashed line) states with no long PEG (black), 8 PEG_{10} (blue), and 8 PEG_{20} (red) is also shown.

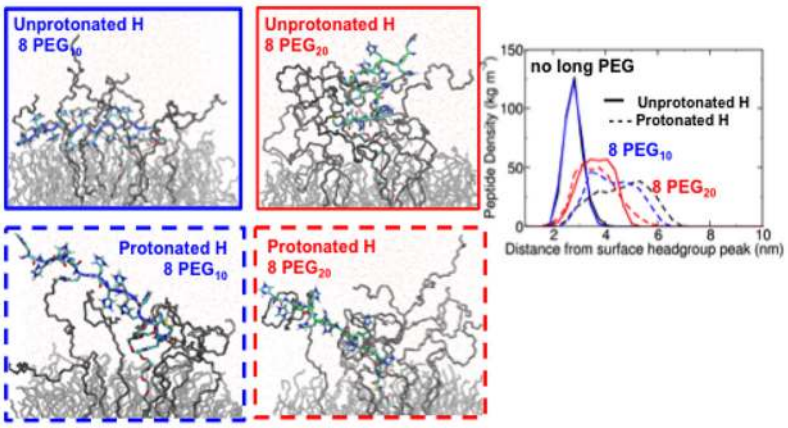

Figure 9.

Representative simulation snapshots of sequence 6 in unprotonated and protonated states. The water and counterions are hidden for clarity, and only a section of the PEG coated substrate is shown. The average peptide density profile, as a function of distance from the PEG surface, for the unprotonated (solid line) and protonated (dashed line) H states with no long PEG (black), 8 PEG_{10} (blue), and 8 PEG_{20} (red) is also shown.

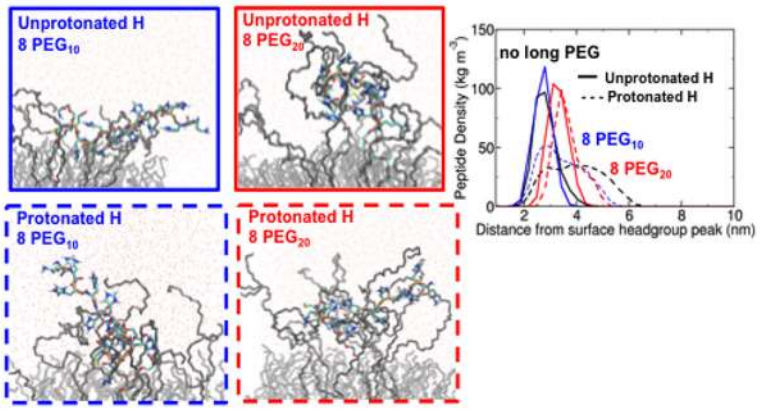

Figure 10.

Representative simulation snapshots of sequence 5a in unprotonated (top row) and protonated (bottom raw) states. The water and counterions are hidden for clarity, and only a section of the PEG coated substrate is shown. The average peptide density profile, as a function of distance from the PEG surface, for the unprotonated (solid line) and protonated (dashed line) states with no long PEG (black), 8 PEG_{10} (blue), and 8 PEG_{20} (red) is also shown.

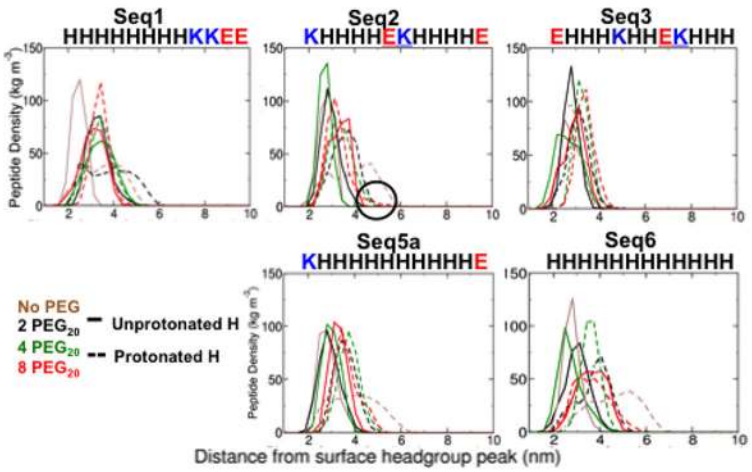

Figure 11.

Average peptide density distribution as a function of distance from the PEG surface for the unprotonated (solid line) and protonated (dashed line) states for the sequence 1, 2, 3, 5a, and 6 with no long PEG (brown), 2 PEG_{20} (black), 4 PEG_{20} (green), and 8 PEG_{20} chains (red).

Table 1

Sequences of the Peptides Used in This Study[a]

Seq1	HHHHHHHHKKEE-C
Seq2	KHHHHEKHHHHE-C
Seq2b	EHHHHEKHHHHK-C
Seq3	EHHHKHHEKHHH-C
Seq4a	KKHHHHHHHHEE-C
Seq4b	EEHHHHHHHHKK-C
Seq5a	KHHHHHHHHHHE-C
Seq5b	EHHHHHHHHHHK-C
Seq6	HHHHHHHHHHHH-C

[a]The residues that undergo protonation with pH change are represented in black (H), the residues with positive charged side chains are represented in blue (K), and the residues with negative charged side chains are represented in red (E).

Table 2

(Upper Table) Average Root Mean Squared End–End Distance, $\langle R_{ee}^2 \rangle^{1/2}$, in nm, for Each Sequence in the Unprotonated and Protonated H States along with the Standard Deviations of the Average Calculated As Described in the Analysis Section;[a] (Lower Table) Average Solvent Accessible Surface Area, ⟨SASA⟩, in Units of Number of 0.14 nm Radius Probes, as a Function of Sequence for Unprotonated and Protonated H States along with the Standard Deviations of the Average Calculated As Described in the Analysis Section

Model	$\langle Ree^2_{\text{Unprot H}} \rangle^{1/2}$ (nm)	$\langle Ree^2_{\text{Prot H}} \rangle^{1/2}$ (nm)	ΔRee (nm)
HHHHHHHHKKEE (Seq1)	1.9 ± 0.19	3.37 ± 0.21	1.46 ± 0.3
KHHHHEKHHHHE (Seq2)	0.79 ± 0.08	3.38 ± 0.24	2.58 ± 0.25
EHHHKHHEKHHH (Seq3)	1.57 ± 0.13	2.74 ± 0.36	1.02 ± 0.31

Model	$\langle SASA \rangle_{\text{Unprot H}}$	$\langle SASA \rangle_{\text{Prot H}}$	ΔSASA
	Units is number of 0.14 nm beads	Units is number of 0.14 nm beads	Units is number of 0.14 nm beads
HHHHHHHHKKEE (Seq1)	710 ± 11	772 ± 13	62 ± 11
KHHHHEKHHHHE (Seq2)	578 ± 19	745 ± 31	167 ± 26
EHHHKHHEKHHH (Seq3)	662 ± 15	738 ± 5	77 ± 16

[a] The ΔR_{ee} between protonated and unprotonated states of H is also shown.

Table 3

(Upper Table) Average Root Mean Squared End–End Distance, $\langle R_{ee}^2 \rangle^{1/2}$, in nm, of Each Sequence for Unprotonated and Protonated States Plus or Minus the Standard Deviations of the Average Calculated As Described in the Analysis Section;[a] (Lower Table) Average Solvent Accessible Surface Area, ⟨SASA⟩, in Units of Number of 0.14 nm Radius Probes, as a Function of Sequence for Unprotonated and Protonated States, Plus or Minus the Standard Deviations of the Average Calculated As Described in the Analysis Section

	NoPEG		2 PEG_{20}		4 PEG_{20}		8 PEG_{20}	
Model	$<Ree^2_{\text{Unprot H}}>^{1/2}$ (nm)	$<Ree^2_{\text{Prot H}}>^{1/2}$ (nm)	$<Ree^2_{\text{Unprot H}}>^{1/2}$ (nm)	$<Ree^2_{\text{Prot H}}>^{1/2}$ (nm)	$<Ree^2_{\text{Unprot H}}>^{1/2}$ (nm)	$<Ree^2_{\text{Prot H}}>^{1/2}$ (nm)	$<Ree^2_{\text{Unprot H}}>^{1/2}$ (nm)	$<Ree^2_{\text{Prot H}}>^{1/2}$ (nm)
HHHHHHHHKKEE (Seq1)	1.9 ± 0.19	3.37 ± 0.21	2.62 ± 0.41	2.88 ± 0.265	3.21 ± 0.39	2.87 ± 0.52	2.61 ± 0.36	0.98 ± 0.2
KHHHHEKHHHHE (Seq2)	0.79 ± 0.08	3.38 ± 0.24	1.27 ± 0.16	0.67 ± 0.21	1.29 ± 0.25	0.79 ± 0.18	0.86 ± 0.13	2.43 ± 0.24
EHHHKHHEKHHH (Seq3)	1.57 ± 0.13	2.74 ± 0.36	1.09 ± 0.13	3.51 ± 0.31	1.14 ± 0.07	1.82 ± 0.14	2.01 ± 0.13	2.68 ± 0.21
KHHHHHHHHHHE (Seq5a)	2.01 ± 0.67	3.37 ± 0.25	2.1 ± 0.45	1.51 ± 0.59	1.4 ± 0.16	1.7 ± 0.41	1.11 ± 0.13	2.67 ± 0.35
HHHHHHHHHHHH (Seq6)	3.31 ± 0.28	3.39 ± 0.39	3.46 ± 0.32	3.18 ± 0.27	3.16 ± 0.45	3.51 ± 0.24	3.31 ± 0.28	3.37 ± 0.29

	NoPEG		2 PEG_{20}		4 PEG_{20}		8 PEG_{20}	
Model	$<SASA>_{\text{Unprot H}}$	$<SASA>_{\text{Prot H}}$	$<SASA>_{\text{Unprot H}}$	$<SASA>_{\text{Prot H}}$	$<SASA>_{\text{Unprot H}}$	$<SASA>_{\text{Prot H}}$	$<SASA>_{\text{Unprot H}}$	$<SASA>_{\text{Prot H}}$
	Units is number of 0.14 nm beads	**Units is number of 0.14 nm beads**	**Units is number of 0.14 nm beads**	**Units is number of 0.14 nm beads**	**Units is number of 0.14 nm beads**	**Units is number of 0.14 nm beads**	**Units is number of 0.14 nm beads**	**Units is number of 0.14 nm beads**
HHHHHHHHKKEE (Seq1)	710 ± 11	772 ± 13	723 ± 27	785 ± 16	753 ± 25	775 ± 17	729 ± 26	711 ± 12
KHHHHEKHHHHE (Seq2)	578 ± 19	745 ± 31	677 ± 45	690 ± 43	735 ± 25	697 ± 24	668 ± 18	758 ± 11
EHHHKHHEKHHH (Seq3)	662 ± 15	738 ± 5	663 ± 8	792 ± 17	631 ± 27	699 ± 27	701 ± 11	765 ± 21

	NoPEG		2 PEG_{20}		4 PEG_{20}		8 PEG_{20}	
Model	**<SASA> Unprot H**	**<SASA> Prot H**	**<SASA> Unprot H**	**<SASA> Prot H**	**<SASA> Unprot H**	**<SASA> Prot H**	**<SASA> Unprot H**	**<SASA> Prot H**
	Units is number of 0.14 nm beads	**Units is number of 0.14 nm beads**	**Units is number of 0.14 nm beads**	**Units is number of 0.14 nm beads**	**Units is number of 0.14 nm beads**	**Units is number of 0.14 nm beads**	**Units is number of 0.14 nm beads**	**Units is number of 0.14 nm beads**
KHHHHHHHHHHE (Seq5a)	662 ± 54	775 ± 15	682 ± 54	716 ± 30	635 ± 20	726 ± 19	688 ± 21	779 ± 26
HHHHHHHHHHHHHH (Seq6)	687 ± 28	789 ± 15	736 ± 24	821 ± 16	702 ± 23	816 ± 22	705 ± 21	809 ± 17

[a]The ΔR_{ee} between protonated and unprotonated states of H is also added.